Effects of Inflow Model on Simulated Aeromechanics of a Quadrotor Helicopter

Robert Niemiec
Graduate Student
Rensselaer Polytechnic Institute
Troy, NY

Farhan Gandhi
Professor
Rensselaer Polytechnic Institute
Troy, NY

ABSTRACT

A dynamic simulation is created for a 2kg quadrotor helicopter, and several inflow models are used to analyze the behavior of the aircraft in trim in hover and forward flight. Intuitive control inputs are derived for a general quadrotor helicopter, and the effects of the inflow model on the required control inputs to achieve steady level flight are analyzed. The inflow models used include a uniform inflow model, Drees' linear inflow model, and the Peters-He generalized dynamic wake model. The flight dynamic modes in hover are also characterized and the effects of the inflow model on their damping and natural frequency are explored.

NOTATION

Ω	Rotor rotational velocity
R	Rotor radius
x	Aircraft x-position (Inertial Frame)
y	Aircraft y-position (Inertial Frame)
z	Aircraft z-position (Inertial Frame)
ϕ	Aircraft roll attitude (Inertial Frame)
θ	Aircraft pitch attitude (Inertial Frame)
ψ	Aircraft yaw attitude (Inertial Frame)
u	Aircraft x-velocity (Body Frame)
v	Aircraft y-velocity (Body Frame)
w	Aircraft z-velocity (Body Frame)
p	Aircraft roll rate(Body Frame)
q	Aircraft pitch rate (Body Frame)
r	Aircraft yaw rate (Body Frame)
V_{hub}	Hub velocity
U_T	Tangential wind velocity
U_P	Perpendicular wind velocity
λ	Inflow Ratio $U_P/\Omega R$
μ	Advance Ratio $V/\Omega R$

INTRODUCTION

Multirotor helicopters are a relatively new configuration for small unmanned aerial systems. They eschew traditional cyclic controls on a single main rotor in favor of smaller, distributed, electrically-driven rotors. Each rotor's speed is allowed to vary, which allows the aircraft to produce the necessary thrust and moments to fly and maneuver. Their mechanical simplicity makes multirotor helicopters easy to build, maintain, and operate, and as such, they are popular among researchers and consumers.

Presented at the AHS 72nd Annual Forum, West Palm Beach, Florida, May 17–19, 2016.

Multirotor helicopters are generally modeled as rigid, six degree of freedom bodies, with the rotors treated as point loads at the ends of the booms. In existing literature, there are several ways these loads have been calculated. Pounds (Ref. 1) used a simple relationship given by equation 1. The proportionality constants a and b are obtained experimentally on a thrust stand, and the factor of $(-1)^i$ accounts for the direction of spin of rotor i. This model neglects all side and drag forces, as well as pitching and rolling moments. Despite these shortcomings, this type of model can be used to control a multirotor helicopter in conditions near hover, as shown by Erginer (Ref. 2) and D'Andrea (Ref. 3). Fay (Ref. 4) used Blade Element Theory (BET) to derive closed-form expressions for the forces and moments on a rotor. This approach assumes linear aerodynamics and uniform inflow, and as such, predicts zero pitching moment and side force on the rotor. This model was used by Bouabdallah and Siegwart (Ref. 5) to develop an obstacle avoidance controller.

$$\begin{aligned} T_i &= a\Omega_i^2 \\ \tau_i &= b\Omega_i^2(-1)^i \end{aligned} \tag{1}$$

This study presents a quadrotor helicopter simulation with a more advanced rotor model. The rotor forces and moments are calculated using BET, but the inflow model used is more sophisticated. The study begins with a description of the dynamic model, and its application in a trim analysis of a quadrotor helicopter using a uniform inflow, and then progresses through more detailed inflow models, including a linear inflow model and a dynamic inflow model. The effects of these models on the trim characteristics is analyzed and explained. The effects of the inflow model on selected flight dynamic modes in hover are also characterized.

SIMULATION DESCRIPTION

To study the behavior of a quadrotor helicopter, a simulation was constructed. The simulation uses the current state of the

aircraft, as well as control inputs to determine forces and moments applied by each component of the aircraft. These forces and moments are resolved about a point located at the centroid of the square defined by the four rotors, and the center of gravity is assumed to be directly below, at a distance z_{cg}.

Basic definitions

The quadrotor helicopter uses two sets of two counter-rotating rotors to achieve trim, with adjacent rotors spinning in opposite directions. The speed of each rotor can be individually controlled to change its thrust and torque. One way to define these controls is the speed of each individual rotor, Ω_N, Ω_S, Ω_E, Ω_W, with the four subscripts denoting the compass directions, north corresponding to the front most rotor. Changing the speed, and thus the load, on any one of the rotors will produce several net forces and moments on the aircraft, each producing a net change in thrust, pitching or rolling moment, and torque. A set of controls that only produce a single force/moment is desirable to obtain an intuitive understanding of the behavior of the quadrotor helicopter. Such a set of controls might be defined as follows: first, we have a "collective RPM" (Ω_0), which provides a baseline rotational speed for all of the rotors - used to adjust the total thrust produced by the rotors. Second, a "differential pitch RPM" ($Omega_P$) increases the rotational speed on the front rotor (Ω_N) and decreases the speed on the aft rotor (Ω_S), causing a nose-up pitching moment. Similarly, "differential roll RPM" (Ω_R) creates a roll-right moment by increasing Ω_W and decreasing Ω_E. Lastly, "differential yaw RPM" (Ω_Y) increases the speed of the rotors spinning counter-clockwise (Ω_N and Ω_S in this simulation) and decreases the speed of the rotors spinning clockwise (Ω_W and Ω_E), inducing a nose-right yawing torque on the aircraft. These controls' effects on the individual rotors are illustrated in Fig. 1, and their overall effects on the aircraft are summarized in Table 1.

The dynamic axes on the system are defined using the north-east-down convention, representing the positive directions for the x-, y-, and z- axes, respectively. This, in turn, defines the direction of positive roll (right), pitch (nose-up), and yaw (nose-right) moments. Forces and moments are considered in two frames: the inertial frame, fixed in space, and the body frame, attached to the body. The positive x-direction is defined as pointing toward rotor N, the positive y-direction is pointing toward rotor E, and the positive z- axis is defined using the right-hand rule. To rotate vectors from one frame to the other, a 3-2-1 Euler angle rotation matrix is used. This matrix is poorly conditioned at pitching angles near 90 degrees, but the aircraft generally avoids such extreme attitudes, so the Euler rotation is well-suited to this simulation.

The simulation is applied to a small quadrotor helicopter, based on the AeroQuad Cyclone ARF kit. This quadrotor helicopter has a takeoff weight of 2 kilograms, and uses four 0.3048m diameter rotors to produce thrust. The booms attached to the fuselage each measure 0.3048m. A NACA 4412 airfoil is used on the inboard section of the rotor, and a Clark Y is used outboard. The aerodynamic characteristics are blended linearly throughout the span.

Rotor Model

The forces produced by each rotor are determined using BET. This theory calculates the forces generated by a blade element located at some radial (r_e) and azimuthal (ψ_b) position, and then integrates over the span of the rotor, and sums over the blades. In trim, rotor forces are averaged over a revolution. The aerodynamic loading on the blade element produces a shear loading at the root as well as a moment. In a conventional rotor, the flapping hinge located near the root of the blade prevents much of this loading from being transferred to the aircraft. A stiff rotor, such as those on a typical quadrotor helicopter, however, readily transmit these moments, and therefore must be accounted for in the analysis.

Each rotor has a rotational velocity Ω, and a direction that is either clockwise or counterclockwise. The azimuthal angle of a rotor blade (ψ_b) is defined to be zero at the aft of the rotor disk, and increases in the direction of rotation. The four rotors are assumed to be identical in their pitch and chord distributions, except for the fact that half are designed to spin clockwise and the other half counter-clockwise. The rotor is assumed to have a linear pitch and chord distribution with root and tip quantities measured from a 12x5.5 APC propeller, and are summarized in Table 2.

On any single blade element, the angle of attack is determined by three parameters: the blade pitch, θ; the tangential velocity, U_T, positive leading edge to trailing edge; and the perpendicular velocity, U_P, positive down. In order to calculate U_T, two effects must be considered. The first, and most obvious, is the rotational speed of the rotor multiplied by the distance from the center of rotation. The other effect is the that of the free-stream velocity on the rotor. The free-stream velocity is measured at the hub, and has three components, given by equation 2.

$$\begin{aligned} V_{hub,x} &= u + Y_i r \\ V_{hub,y} &= v + X_i r \\ V_{hub,z} &= w - Y_i p - X_i q \end{aligned} \tag{2}$$

where X_i and Y_i are, respectively, the x- and y-coordinate of rotor i, and have units of length.

U_P has three major contributors: the first is the induced velocity λ_i, the second is the vertical travel of the hub, and the third is travel due to rotation about the hub. U_T and U_P at any blade element are given by equation 3. In general, λ_i is a function of blade azimuth and radial location, and the shape of this function and its effects on the aeromechanics of a quadrotor helicopter is the focus of this study.

$$\begin{aligned} U_T &= \Omega r_e + V_{hub,x} \sin\psi_b + (-1)^k V_{hub,y} \cos\psi_b \\ U_P &= \Omega R \lambda_i + V_{hub,z} - (-1)^k r_e p \sin(\psi_b) - r_e q \cos(\psi_b) \end{aligned} \tag{3}$$

where $k = 0$ for rotors spinning counterclockwise, and $k = 1$ for rotors spinning clockwise.

The angle of attack is given by equation 4 (Ref. 6). From the angle of attack and incident velocity, the elemental lift and drag can be calculated using equation 6.

$$\alpha = \theta - \phi_i \tag{4}$$

$$\phi = \tan^{-1}\frac{U_P}{U_T} \tag{5}$$

$$\begin{aligned} dL &= \frac{1}{2}C_l(\alpha, r_e)\rho(U_T^2 + U_P^2)c dr_e \\ dD &= \frac{1}{2}C_d(\alpha, r_e)\rho(U_T^2 + U_P^2)c dr_e \end{aligned} \tag{6}$$

The lift and drag are perpendicular and tangential to the incident velocity, respectively, so in order to resolve the forces normal and tangential to the rotor disk, the vectors must be rotated by ϕ (Equation 7).

$$\begin{aligned} dF_z &= dL\cos\phi_i - dD\sin\phi_i \\ dF_x &= -dL\sin\phi_i + dD\cos\phi_i \end{aligned} \tag{7}$$

The blade element's contribution to the rotor lift is given by equation 8. H is the rotor drag, acting in the x-direction (positive forward), T is the thrust oriented normal to the rotor plane (positive down), and Y is the side force (positive right). Its contribution to the moment is given by equation 9. M_x is a rolling moment, positive roll-right, M_y is the pitching moment, positive nose-up, and M_z is the rotor torque, positive nose-right.

$$\begin{aligned} dH &= -dF_x\sin\psi_b \\ dY &= -(-1)^k dF_x\cos\psi_b \\ dT &= -dF_z \end{aligned} \tag{8}$$

$$\begin{aligned} dM_x &= -(-1)^k dF_z r_e\sin\psi_b \\ dM_y &= -dF_z r_e\cos\psi_b \\ dM_z &= (-1)^k dF_x r_e \end{aligned} \tag{9}$$

To get the average overall rotor forces, the element forces are integrated along the radius on each blade, and then summed across the number of blades. In trim, the forces are instead averaged across a revolution, so equation 10 is the expression for the rotor thrust used for trim analysis.

$$T = \frac{N_b}{2\pi}\int_0^{2\pi}\int_0^R T(R,\psi)dRd\psi \tag{10}$$

The rigid body equations of motion expressed in the body frame are given by equation 11. In this simulation, the magnitudes of p, q, and r are assumed to be small, and the net angular momentum of the rotors is also close to zero, since the momentum of the clockwise rotors cancels out with that of the counter-clockwise motors. Therefore, the gyroscopic moments are small, and are neglected. To track the position and velocity as well as the attitudes, a total of 12 rigid body states are needed.

$$\begin{aligned} m\dot{u} &= D_{fuse,x} - g\sin(\theta) + \sum_{i=1}^{4} H_i \\ m\dot{v} &= D_{fuse,y} - g\sin(\phi)\cos(\theta) + \sum_{i=1}^{4} Y_i \\ m\dot{w} &= D_{fuse,z} + g\cos(\phi)\cos(\theta) + \sum_{i=1}^{4} T_i \\ I_{xx}\dot{p} &= -z_{cg}mg\sin(\phi)\cos(\theta) + \sum_{i=1}^{4}(M_{x_i} + T_i Y_i) \\ I_{yy}\dot{q} &= -z_{cg}mg\sin(\theta) + \sum_{i=1}^{4}(M_{y_i} + T_i X_i) \\ I_{zz}\dot{r} &= \sum_{i=1}^{4}(M_{z_i} + Y_i X_i - H_i Y_i) \end{aligned} \tag{11}$$

Inflow Models

Due to conservation of momentum, any thrust generated by a rotor also induces a change in momentum of the air surrounding it. The structure of the inflow distribution over the rotor disk is crucial to the determination of forces and moments produced by the rotor. The simplest inflow model is known as uniform inflow (equation 12), which, true to its name, assumes that the inflow distribution is constant across the disk. The magnitude of the inflow ratio is given by momentum theory and shown in equation 13 (Ref. 6).

$$\lambda(r_e, \psi_b) = \frac{U_P(r_e, \psi_b)}{\Omega R} = \lambda_0 \tag{12}$$

$$\lambda_0 = \mu_x\tan\alpha + \frac{C_T}{2\sqrt{\mu_x^2 + \lambda_0^2}} + \mu_z \tag{13}$$

Uniform inflow models work well in hover, but are usually inaccurate in forward flight. The next step is to allow linear variation in the inflow. Linear inflow models take the form shown in equation 14. Many models of k_x and k_y exist. One such model is the Drees model (Ref. 7), described in equation 15, with λ_0 given by equation 13.

$$\lambda(r_e, \psi_b) = \lambda_0(1 + k_x r_e\cos\psi_b + k_y r_e\sin\psi_b) \tag{14}$$

$$\begin{aligned} k_x &= \frac{4}{3}\left(\frac{1 - \cos\chi - 1.8\mu_x^2}{\sin\chi}\right) \\ k_y &= -2\mu_x \\ \chi &= \tan^{-1}\left(\frac{\mu_x}{\mu_z + \lambda_i}\right) \end{aligned} \tag{15}$$

The third inflow model considered in this paper is the Peters-He model (Ref. 8). This is a generalized dynamic wake model, with first-order dynamics in the inflow states. The induced inflow distribution is given by equation 16. ϕ_n^m is a polynomial of order $n-1$ and describes a mode of radial variation of inflow. Relevant ϕ_m^n are plotted in figure 2. The parameter m indicates the frequency of the harmonic variation of the inflow as the blade rotates azimuthally. For each $n = m+1, m+3, \ldots$ when $m > 0$, there are two associated states: α_n^m and β_n^m. When $m = 0$, there is only one state for each $n = 1, 3, 5, \ldots$: α_n^0. When the sum in equation 16 is truncated by limiting m and n to values less than or equal to r and j, respectively, the model is referred to as an $r \times j$ Peters-He model. The two cases primarily considered in this study are a 0x1 (1 state) model, where the inflow distribution is uniform, and a 1x2 model (3 states), where the distribution is linear.

$$\lambda_i = \sum_{m=0}^{\infty} \left(\sum_{n=m+1,m+3,\ldots}^{\infty} \phi_n^m(\bar{r}) \left[\alpha_n^m(\bar{t}) \cos(m\psi_b) + \beta_n^m(\bar{t}) \sin(m\psi_b) \right] \right) \tag{16}$$

where $\bar{r} = \frac{r_e}{R}$ and $\bar{t} = \Omega t$ are normalized radial position and time.

An important feature of the Peters-He inflow model is that the derivatives of the inflow can be defined as a function of the lift distribution by equation 17. Equation 17 is a matrix equation which is the same size as the number of states used. Each rotor, since they generally operate at different speeds, will each have their own inflow states, so the total number of equations of motion associated with inflow is four times the number of states per rotor.

$$\begin{aligned} \Omega[K_m^{nc}]\{\dot{\alpha_n^m}\} + V[\bar{L}_s]^{-1}\{\alpha_n^m\} &= \frac{1}{2}\{\tau_n^{mc}\} \\ \Omega[K_m^{nc}]\{\dot{\beta_n^m}\} + V[\bar{L}_s]^{-1}\{\beta_n^m\} &= \frac{1}{2}\{\tau_n^{ms}\} \end{aligned} \tag{17}$$

where

$$\{\tau_n^{0c}\} = \frac{1}{2\pi} \sum_{q=1}^{n_{blades}} \int_0^1 \frac{L}{\rho\Omega^2 R^3} \phi_n^0(\bar{r}) d\bar{r}$$

$$\{\tau_n^{mc}\} = \frac{1}{\pi} \sum_{q=1}^{n_{blades}} \int_0^1 \frac{L}{\rho\Omega^2 R^3} \phi_n^m(\bar{r}) d\bar{r} \cos(m\psi_q)$$

$$\{\tau_n^{ms}\} = \frac{1}{\pi} \sum_{q=1}^{n_{blades}} \int_0^1 \frac{L}{\rho\Omega^2 R^3} \phi_n^m(\bar{r}) d\bar{r} \sin(m\psi_q)$$

In trim, the forcing functions are averaged over a rotor revolution to determine the inflow distribution.

TRIM ANALYSIS

The equations of motion (11) of the quadrotor helicopter are solved for the four control inputs defined in figure 1 as well as the pitch and roll attitude needed to maintain steady-level flight at speeds ranging from hover to 15 m/s. When the Peters-He model is used, the inflow states, α_m^n and β_m^n, are also solved using equation 17 such that their time derivatives are zero.

Uniform Inflow

The required trim controls to maintain trim as a function of aircraft speed are shown in figure 3. The required collective RPM falls with forward speed until it reaches a minimum at 7 m/s (Fig. 3, top left). The reduction occurs because forward flight reduces the induced inflow ratio, increasing the efficiency of the rotor. At higher speeds, the thrust required to overcome drag increases dramatically, and so the collective RPM increases. The pitch attitude begins at zero in hover and increases nose-down with forward speed, as the thrust vector must be tilted increasingly forward in order to overcome drag (Fig. 3, bottom left). The center of gravity, located below the rotor plane, causes a restoring (nose up) pitching-moment, which must be counteracted by (negative) differential pitch RPM (Fig. 3, top-right).

Without cyclic pitch control, a rotor outside of axial flight is loaded asymmetrically, as the advancing blades experience a higher dynamic pressure than the retreating blades. Therefore, a rolling moment exists on the rotor in forward flight, and is transmitted to the aircraft. However, the fact that two rotors are spinning counterclockwise while the other two are spinning clockwise cause these moments to act in opposite directions relative to one another (advancing blades produce a roll-left moment on the CCW rotors, and a roll-right moment on the CW rotors), so that the net moment on the aircraft, and thus the roll control effort required, is approximately zero. Despite canceling out at the aircraft level, the roll moments must be borne by the booms supporting the rotors, where it will appear as a twisting moment (for the north and south rotor) or an out-of-plane bending moment (for the east and west rotor).

Similarly, the torques due to profile and induced drag on the counter-clockwise rotors counteract those on the clockwise rotors. Yawing torque due to rotor drag on the east and west rotors is canceled by the virtue that the two rotors are on opposite sides of the origin, and spin at the same speed (a consequence of zero differential roll input). The assumption of uniform inflow causes a symmetry between the front and aft of the rotor disk, and so there can be no net side force out of any rotor, implying that there is no resulting yawing torque produced by the north and south rotors. Thus, the required differential yaw input is also approximately zero. Again, these torques must be borne by the booms, which will manifest as an in-plane bending moment.

Linear Inflow

The required trim controls to maintain trim using Drees' linear inflow model as a function of aircraft speed are shown in figure 4. The required collective RPM is largely unchanged

from the uniform inflow case, as is the required pitch attitude. This is intuitive, as the total thrust is largely governed by the mean inflow, which is calculated the same way, and the total drag on the aircraft is similar with both inflow models. The steady-state inflow parameters of equation 14 for each rotor as a function of the speed are shown in Figure 5. The longitudinal distribution in forward flight is such that the front of the disk experiences less downwash than the aft of the disk, and the lateral distribution is such that the advancing side sees less downwash than the retreating side. The inflow distribution is illustrated in Fig. 6.

The most striking difference between the predicted controls is seen in the required differential pitch RPM. The uniform inflow model underpredicts the required control input by more than 80% at 15 m/s, relative to the linear inflow model. The source of the disparity can be traced directly to the inflow distribution. The longitudinal inflow distribution increases the angle of attack on the front of the rotor disk, and reduces it on the aft of the disk, thereby affecting the lift distribution. Figure 7 shows a comparison between the lift distributions on the front rotor using uniform (top) and linear (bottom) inflow models. In the former case, the lift is symmetric about the 90° - 270° line, and in the latter case, the lift is biased toward the front of the disk, producing a net nose-up moment on the rotor. This effect, unlike the advancing-blade effect, is independent of the direction of rotor spin, and thus compounds across the four rotors. The net effect is a large aerodynamic pitching moment, which must be compensated by negative differential pitch RPM (Fig. 4, top right).

Unlike the uniform inflow case, there is a net side force on each rotor. Again, the longitudinal inflow distribution is the cause. Higher inflow on the aft of the disk increases induced drag on the aft of the rotor disk, while induced drag is reduced on the front of the disk. The distribution of Y-force on the south rotor disk is pictured in Fig. 8. A large region of high drag on the aft of the advancing side of the south rotor disk results in a net side force to the left. Though the net Y-force on the aircraft is still approximately zero (The clockwise rotors counteracting the counterclockwise rotors), the side force on the north and south rotors each produce a yawing moment in opposite directions. However, since the aft rotor produces more force, it "wins" and the net effect is a nose-right (positive) moment on the aircraft. The east and west rotors also produce a side force, but these have no moment arm by which to produce a yawing moment (Fig. 9). This moment is countered by the introduction of (negative) differential yaw RPM (Fig. 4, center-right).

An interesting feature of the differential yaw RPM curve is the curvature it exhibits, leading to a change in sign close to 15 m/s. This coincides with a change in the resultant Y-force produced by the rotors (Fig. 10). When the Y-force produced by the south rotor is more negative than that produced by the north rotor, the aircraft experiences a nose-right moment. This is the case when the aircraft speed is less than 13 m/s (The intersection point in Fig. 10). Thereafter, the Y-force on the aft rotor is more positive than on the front rotor, inducing a nose-left moment.

The introduction of differential yaw RPM has the secondary effect of producing a rolling moment in forward flight. This is due to the advancing blade effect. When negative differential yaw RPM is applied, the thrust produced by both the north and south rotors decreases, which, in turn, reduces the roll-left moment produced (Fig. 11). Conversely, the thrust produced by the east and west rotors increases, which increases their roll-right moment. The net effect is to produce a roll-right moment, which must be compensated by negative differential roll RPM.

Peters-He Inflow

The required trim controls using a 1x2 (3 state) Peters-He inflow model are presented in figure 12. This inflow model are qualitatively similar to Drees inflow, since they both model the inflow with a linear distribution, so the required trim controls are also qualitatively similar. In addition to using the trim controls to bring the accelerations of the aircraft to zero, the inflow distribution on each rotor is solved such that it is also steady in time. Using the three inflow states, it is possible to describe the distribution in the form of equation 14, whose steady-state parameters are plotted as a function of flight speed in Figure 13. Notably, the sign on k_y is opposite that predicted by Drees' model, predicting additional downwash on the advancing side of the rotor disk, instead of hte retreating side. This is due to the fact that in the Peters-He model, the inflow is directly related to the lift distribution on the rotor. A higher lift, as seen on the advancing side, corresponds to greater inflow in that region. Drees' model does not capture this effect on a fixed-pitch rotor, since it was developed for an articulated rotor with cyclic pitch inputs. Relative to Drees' model, the Peters-He will predict less rolling moment produced by the rotor, as the lateral inflow variation serves to mitigate the differences due to dynamic pressure variation, while Drees' model enhances them. Though the effects on the lateral distribution are largely canceled out at the aircraft level, the loads at the rotor level will be different, which will affect the loads borne by the airframe. This being the case, Drees' model is not recommended for the modeling of fixed-pitch rotors.

The power requirements of the quadrotor helicopter using three inflow models (Uniform, Drees, and 1x2 Peters-He) are plotted as a function of speed in figure 14. The power is almost entirely governed by collective RPM, since the other three controls reduce power on as many rotors as they increase power, and so the power curves for uniform and Drees inflow are practically identical. Since the collective RPM prediction using the 1x2 Peters-He models is greater, the predicted power is also higher.

It is possible to allow for more inflow states with the Peters-He model. For example, the required trim controls when using a 2x3 (6 state), 3x4 (10 state), and 4x5 (15 state) Peters-He model are given by Fig. 15, and the required power is shown in Fig. 16. Going from the 3 state model to the 6 state model significantly changes the predicted differential pitch RPM requirements, bringing them between the uniform

inflow case and the 3 state model, which is a result of lowered pitching moments coming from the rotors, illustrated by the lift distribution along the 0° - 180° line in Fig 17. The 0x1 (blue in Fig. 17) inflow case shows that lift is symmetric between the front and aft of the disk, and that the 1x2 (red) case shows a relative increase in lift on the front of the disk and a loss of lift on the aft. Higher order inflow models show a recovery of lift on the aft of the disk, and a reduction in lift on the front, though it is still higher than the 0x1 case. Lift over the whole rotor in Fig. 18, and the rest of the disk follows a similar trend as the 0° - 180° line. The inflow distribution is also more uniform, particularly on the inboard section of the rotor (Fig. 19). The predicted collective pitch requirements are also reduced compared to the 1x2 Peters-He model. The 3x4 and 4x5 Peters-He agree in terms of control (Fig. 15) and power requirement (Fig. 16), with values slightly different than the 2x3 Peters-He.

Takeaways

The required trim controls are expected to vary significantly with the inflow model used. Most importantly, the required differential pitch RPM increases drastically when longitudinal variation in inflow is allowed, which increases (reduces) thrust on the front (aft) of the rotor disk, inducing a net pitching moment. Also, the introduction of linear inflow requires the use of control inputs not predicted by uniform inflow. Higher order Peters-He inflow models predict greater differential pitch RPM than the uniform case, but not to the same degree as the 1x2 Peters-He or Drees models do. All told, the inflow model has a strong effect on the trim behavior of the quadrotor helicopter, and a uniform inflow model is insufficient to capture all of the moments and forces produced by a fixed-pitch rotor.

In all cases, the collective RPM is on the order of 10^3 RPM, and thus a period on the order of 10^{-2} seconds. Because the rotor is spinning so quickly, it is reasonable to continue using the average rotor forces over a revolution as the instantaneous force when simulating the dynamics of the aircraft, as long as the time scale of body motion is large compared to the period of the rotors.

DYNAMIC MODELING

To analyze the dynamic behavior of the quadrotor helicopter, a state-space representation of the nonlinear system is generated. A state-space model is a linear approximation of the nonlinear model and takes the form of equation 18.

$$\begin{aligned} \dot{\vec{x}} &= A\vec{x} + B\vec{u} \\ \vec{y} &= C\vec{x} + D\vec{u} \end{aligned} \tag{18}$$

where

$$A \in \mathbb{R}^{n\times n} \qquad B \in \mathbb{R}^{n\times n_c}$$
$$C \in \mathbb{R}^{n_o\times n} \qquad D \in \mathbb{R}^{n_0\times n_c}$$

where n is the number of dynamic states (12 for uniform or Drees' inflow models, 24 for the 1x2 Peters-He inflow model), n_c is the number of control inputs (4, see Fig. 1), and n_o is the number of outputs to be tracked. These outputs can be any linear combination of states and control inputs; for this simulation, $C = \mathbb{1}$, and $D = \mathbb{0}$, implying that $\vec{y} = \vec{x}$. In order to approximate the nonlinear function, the matrices A and B should take the form of equation 19.

$$A = \begin{bmatrix} \frac{\partial \dot{x}_1}{\partial x_1} & \frac{\partial \dot{x}_1}{\partial x_2} & \cdots & \frac{\partial \dot{x}_1}{\partial x_n} \\ \frac{\partial \dot{x}_2}{\partial x_1} & \frac{\partial \dot{x}_2}{\partial x_2} & \cdots & \frac{\partial \dot{x}_2}{\partial x_n} \\ \vdots & \vdots & \ddots & \vdots \\ \frac{\partial \dot{x}_n}{\partial x_1} & \frac{\partial \dot{x}_n}{\partial x_2} & \cdots & \frac{\partial \dot{x}_n}{\partial x_n} \end{bmatrix}$$

$$B = \begin{bmatrix} \frac{\partial \dot{x}_1}{\partial u_1} & \frac{\partial \dot{x}_1}{\partial u_2} & \cdots & \frac{\partial \dot{x}_1}{\partial u_{n_c}} \\ \frac{\partial \dot{x}_2}{\partial u_1} & \frac{\partial \dot{x}_2}{\partial u_2} & \cdots & \frac{\partial \dot{x}_2}{\partial u_{n_c}} \\ \vdots & \vdots & \ddots & \vdots \\ \frac{\partial \dot{x}_n}{\partial u_1} & \frac{\partial \dot{x}_n}{\partial u_2} & \cdots & \frac{\partial \dot{x}_n}{\partial u_{n_c}} \end{bmatrix} \tag{19}$$

The derivatives in equation 19 are estimated numerically using centered finite differences. These linear models are generated about a trim condition, so that the control input required to maintain trim is defined as $\vec{u} = \mathbb{0}$, and the trim condition is defined as $\vec{x} = \mathbb{0}$.

To assess the natural behavior of the aircraft about its trim condition, $\vec{u}$ in equation 18 is set to zero. Therefore, the autonomous system can be described as $\dot{\vec{x}} = A\vec{x}$. The dynamic modes of this system are the eigenvectors of A. Regardless of the inflow model or flight condition, there are 12 poles associated with the body, three of which are simple integrators associated with the position of the aircraft; these states have no effect on the accelerations of the aircraft (altitude effects are neglected). The remaining 9 poles are dependent on the inflow model and flight condition. When using the 1x2 Peters-He inflow model, there are an additional 12 poles associated with the inflow states, but these poles have very large negative real components. For comparison, linear models using a 0x1 Peters-He dynamic inflow model are also constructed.

In hover, there is one additional integrator associated with the heading of the aircraft, which like position, has no effect on accelerations in hover. There are several other real poles of the linear systems, corresponding to heave motion, lateral and longitudinal translation, and spinning of the aircraft about the z-axis. Due to symmetry of the aircraft in hover, the translation modes have identical eigenvalues. The time constants of these modes under the different inflow models is illustrated in figure 20.

The heave mode (Fig. 20, left) arises when the aircraft experiences a vertical perturbation, and is damped by the change in the mean inflow induced by ascent or descent, and is very stable for all inflow cases. The translation mode (Fig 20, center) is relatively poorly damped in the uniform inflow cases,

since the only source of damping is drag on the fuselage and rotors. When a linear inflow model is used, attitude coupling increases the damping of this mode. The yaw mode (Fig. 20, right) is the most poorly damped mode in hover, with time constants on the order of 10 seconds, and is characterized by the aircraft rotating about its own z-axis. It is damped only by aerodynamic drag on the rotors.

In addition to the real poles, there are two complex poles in hover, one in the longitudinal direction, and one in the lateral direction. Again, because of the symmetry of the craft in hover, these modes have identical eigenvalues in hover. Each of these modes couples translation and rotation in an an oscillatory fashion, and are referred to as the longitudinal phugoid mode and lateral phugoid mode. The longitudinal phugoid mode in hover is illustrated in figure 21. A nose-down pitch attitude, [1], causes the aircraft to fly forward. At the same time, the quadrotor experiences a nose-up pitching moment, and begins to rotate accordingly through [2-4]. The aircraft thus flies forward until it reaches a maximum displacement at [5]. The nose-up attitude causes the aircraft to then fly backwards through [6-8] until it returns to [1]. The position of the aircraft on the return is shown in the offset boxes in figure 21, but there is no vertical travel, and the position of the quadrotor at [6,7, and 8] is the same as in [4, 3, and 2], respectively.

The damping ratio and damped natural frequency of these modes is illustrated in Fig. 22. From Fig. 22, it is clear that while the natural frequency is not very sensitive to the inflow model, the damping ratio varies significantly. The damping ratio is strongly influenced by pitching moments associated with translation and rotation. There are three major contributors to the pitching moment. The first, present with all inflow models, is a restoring moment produced by gravity when the aircraft pitches. Since the CG is beneath the origin of the body frame, a pitch attitude causes a component of gravity to act in the x-direction and produce a restoring pitching moment. The second, also present in all cases, is a damping moment caused by vertical travel of the rotors. When the quadrotor has a nose-up pitch rate, for example, the front rotor is put into climb, and the aft rotor into descent. The relative velocity causes an increase in the lift produced by the aft rotor, and a decrease in the front, producing a nose-down moment. The third moment is a pitching moment due to forward velocity. This moment comes about due to the longitudinal inflow distribution, which is obviously not present in the uniform inflow case. Forward velocity causes a strong nose-up pitching moment, and this reduces the damping ratio of the phugoid mode, as seen in figure 22. Use of the dynamic inflow models increases damping dramatically whether the distribution is uniform or linear in nature. The damping ratio converges quickly as the number of inflow states increases, converging to a value between the 0x1 Peters-He and 1x2 Peters-He (Fig. 23).

CONCLUSIONS

A dynamic simulation of a quadrotor helicopter was developed around Blade Element Theory, and the effects of the inflow model used on the trim and dynamic behavior of the aircraft were predicted. Using a linear inflow model yielded much higher predictions for the differential pitch RPM required in forward flight, and predicted nonzero differential roll and yaw RPM in trim, which the uniform inflow model could not capture. Use of the Peters-He finite-state dynamic inflow model showed that the lateral distribution of inflow is not that predicted by Drees' model, which was developed for a conventional rotor. This difference means little to the overall trim behavior of the aircraft, but may be important to the loads borne by the hubs and booms attached to the rotors.

The dynamic behavior of the quadrotor helicopter was also modeled with various inflow types. The hover modes have been identified and the effects of the inflow model on them are described. Use of linear inflow models causes the phugoid modes to become less stable, and adding dynamic inflow increases damping. Higher order inflow models further increase the predicted damping in the longitudinal (and lateral) phugoid mode.

Author contact: Robert Niemiec, niemir@rpi.edu; Farhan Gandhi - Corresponding Author, fgandhi@rpi.edu

ACKNOWLEDGMENTS

The first author gratefully acknowledges the National Defense Science and Engineering Graduate (NDSEG) Fellowship support for his graduate studies at RPI.

REFERENCES

[1]Pounds, P., "Design of a Four-Rotor Aerial Robot," 2002 Australasian Conference on Robotics and Automation, Auckland, Australia, November 27–29, 2002

[2]Erginer, B., Altuğ E., "Modeling and PD Control of a Quadrotor Vehicle," 2007 IEEE Intelligent Vehicles Symposium, Istanbul, Turkey, June 13–15, 2007

[3]Mueller, M., D'Andrea, R., "Stability and control of a quadrocopter despite the complete loss of one, two, or three propellers," 2014 IEEE International Conference on Robotics and Automation, Hong Kong, China, May 31 – June 7, 2014

[4]Fay, G. "Derivation of the aerodynamic forces for the mesicopter simulation," Stanford University, CA, 2001

[5]Bouabdallah, S., Siegwart, R., "Full Control of a Quadrotor," 2007 ISEE/RSJ International Conference on Intelligent Robots and Systems, San Diego, CA, October 29 – November 2, 2007.

[6]Leishman, J. G., *Principles of Helicopter Aerodynamics*, Cambridge University Press, New York, NY, 2000, Chapter 2-3.

[7]Drees, J. M. Jr., "A Theory of Airflow Through Rotors and its Application to Some Helicopter Problems", *Journal of the Helicopter Association of Great Britain*, Vol. 3, No. 2, July–Sept 1949, pp. 79–104.

[8]Peters, D., He, C., "A finite-state induced-flow model for rotors in hover and forward flight," 43rd Annual National Forum of the American Helicopter Society, St. Louis, MO, May 1987.

FIGURES AND TABLES

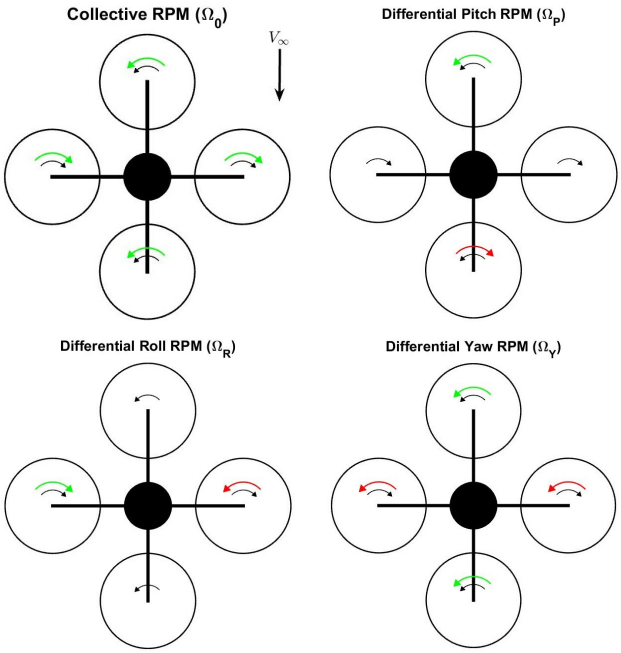

Fig. 1. Control Definition

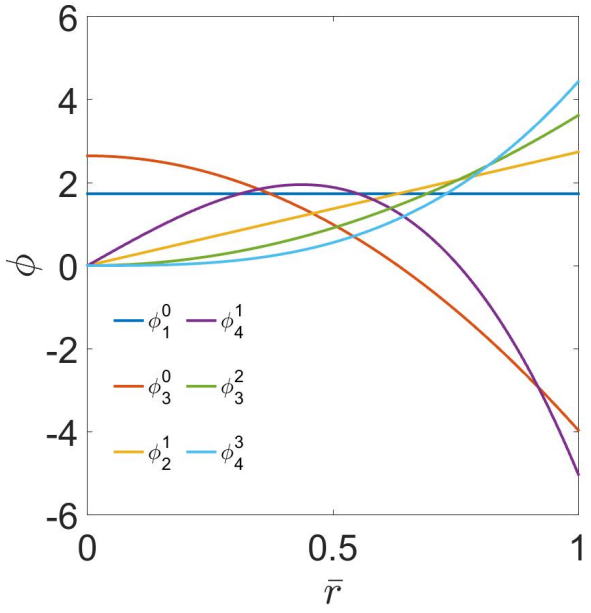

Fig. 2. Radial inflow shape functions

Table 1. Controls of a quadrotor helicopter

Rotor	Collective RPM	Diff. Pitch RPM	Diff. Roll RPM	Diff. Yaw RPM
North	$+1$	$+1$	0	$+1$
West	$+1$	0	$+1$	-1
South	$+1$	-1	0	$+1$
East	$+1$	0	-1	-1
Effect	More Thrust	Nose Up	Roll Right	Nose Right

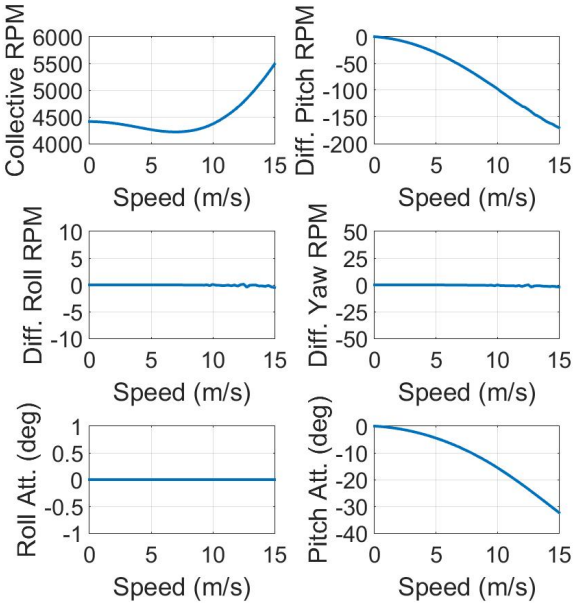

Fig. 3. Predicted Trim Solution - Uniform Inflow

Table 2. Blade Geometry

	Pitch (deg)	Chord (m)
Root	21.5	0.031
Tip	11.1	0.012

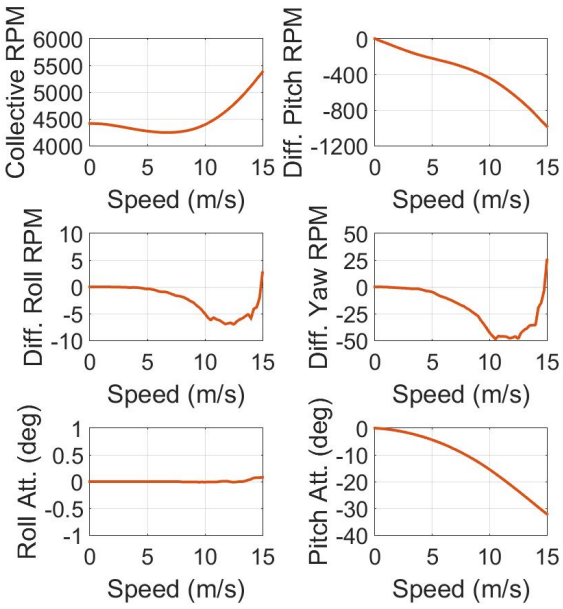

Fig. 4. Predicted Trim Solution - Linear Inflow

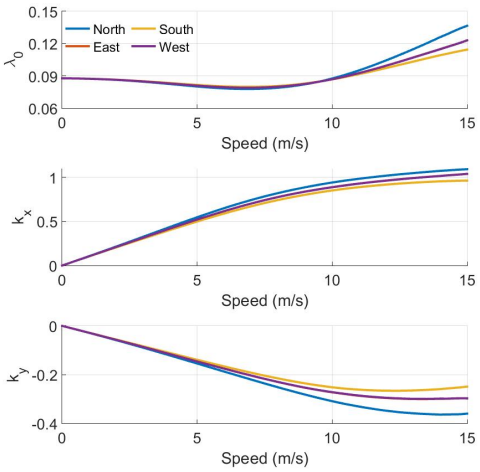

Fig. 5. Inflow Parameters - Drees' Model

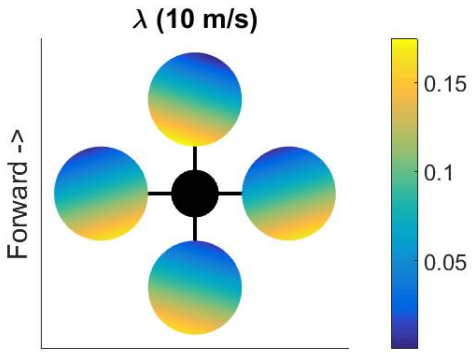

Fig. 6. Inflow distribution - Linear Inflow

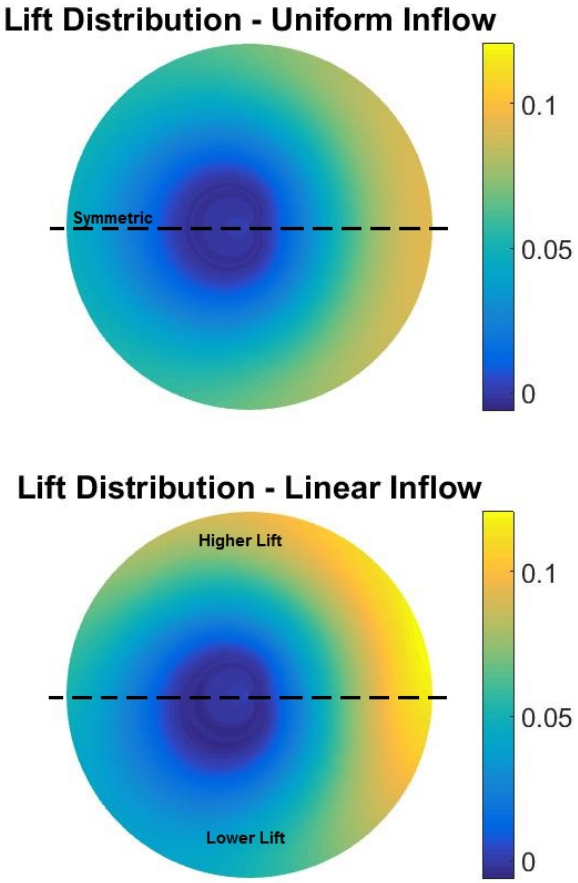

Fig. 7. Lift distribution on front rotor at 10 m/s

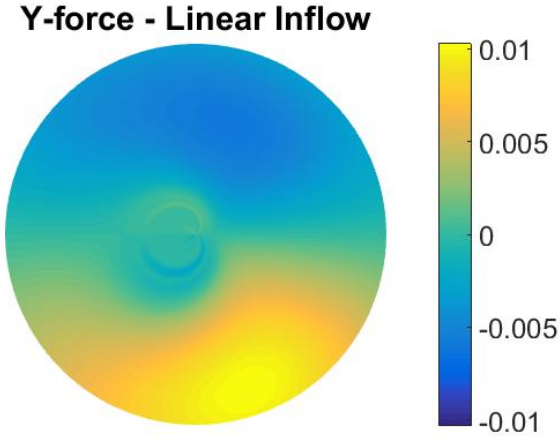

Fig. 8. Y-force distribution aft rotor at 10 m/s

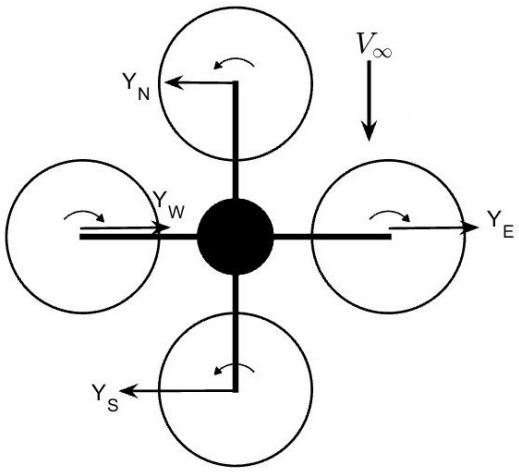

Fig. 9. Side forces on Quadrotor Helicopter

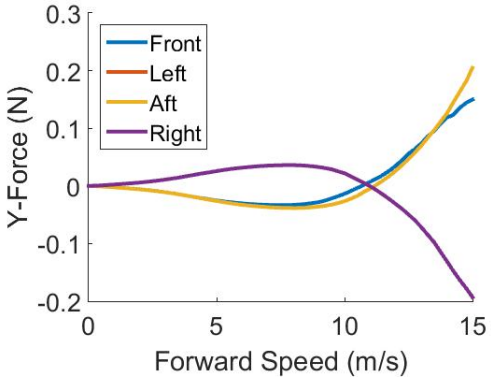

Fig. 10. Integrated Y-force on the four rotors - Linear Inflow

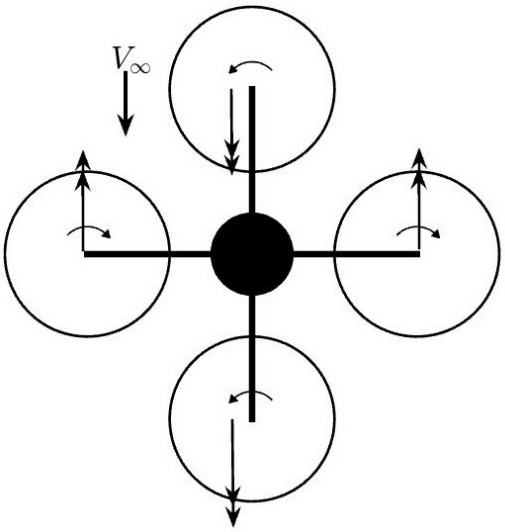

Fig. 11. Roll Moments on Quadrotor Helicopter

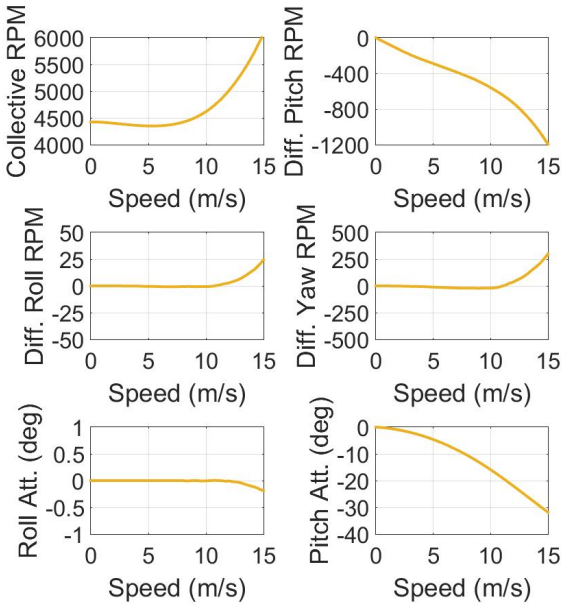

Fig. 12. Predicted Trim Solution - Dynamic Inflow

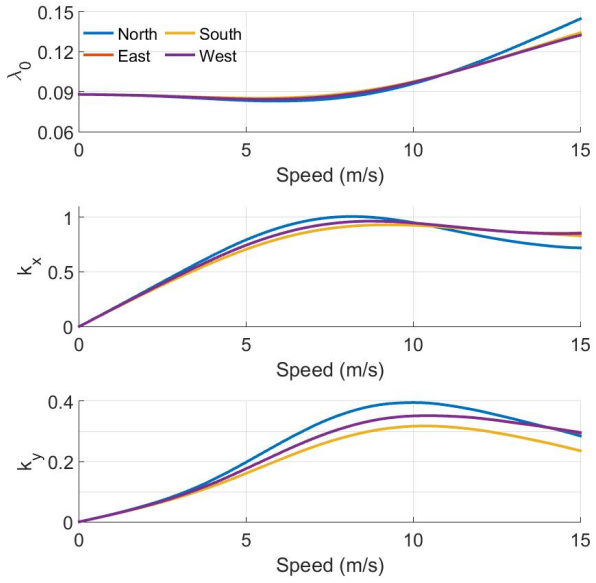

Fig. 13. Inflow Parameters 1x2 Peters-He Model

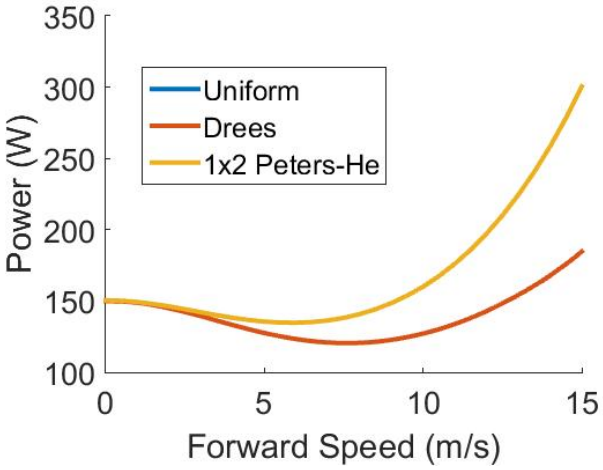

Fig. 14. Power Requirements in trimmed flight

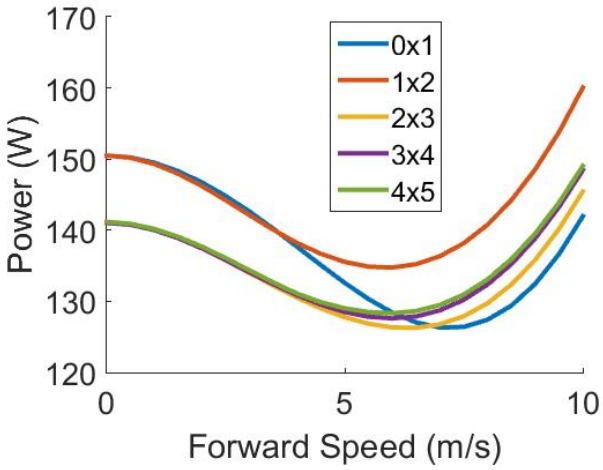

Fig. 16. Power Requirements predicted using Peters-He inflow models

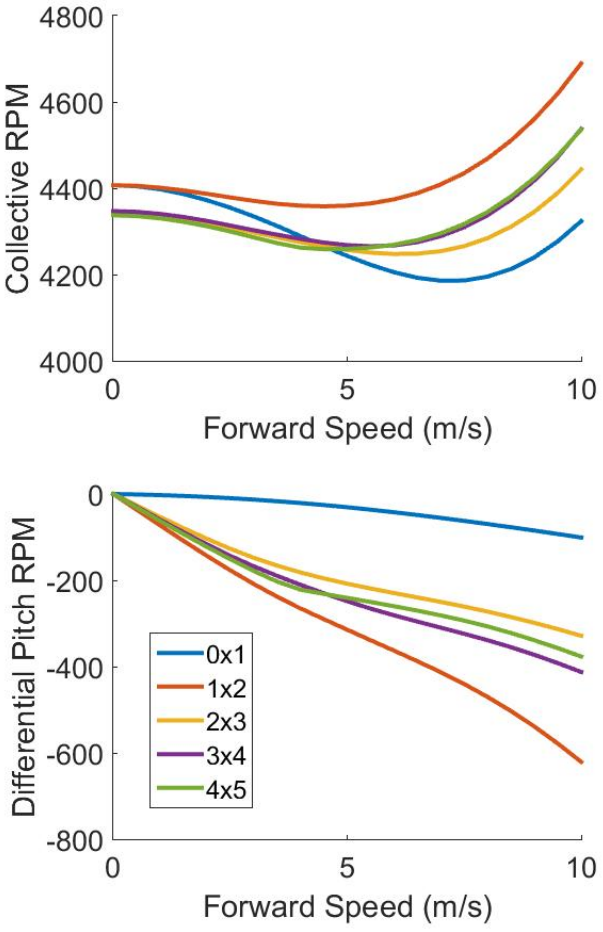

Fig. 15. Collective and Pitch RPM controls using Peters-He inflow models

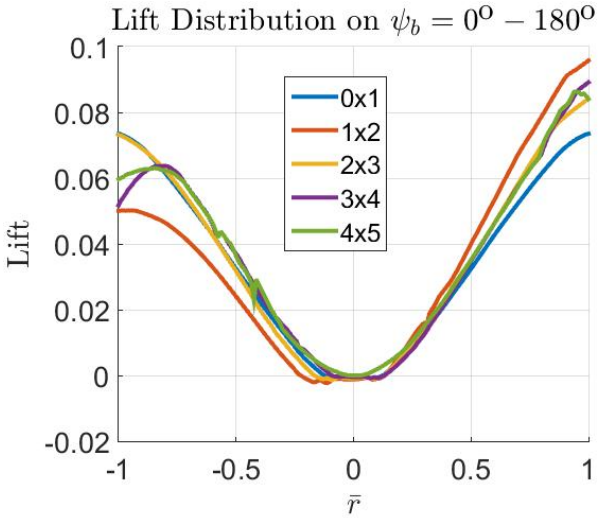

Fig. 17. Longitudinal Lift Distribution on the north rotor at 10 m/s

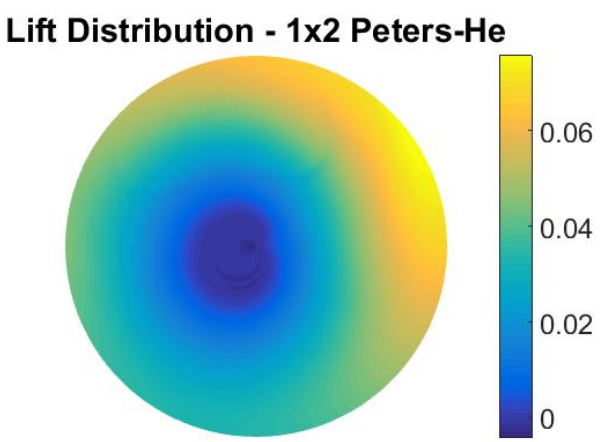

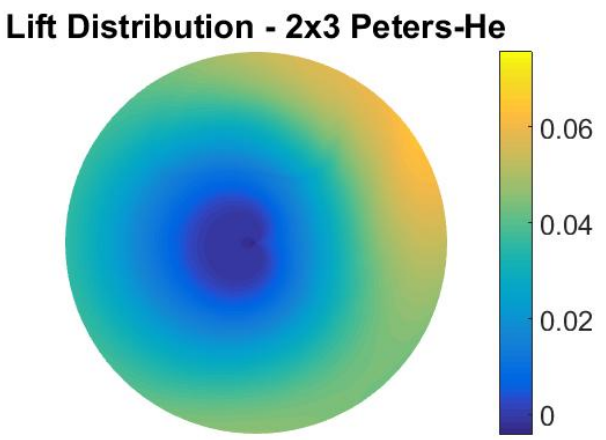

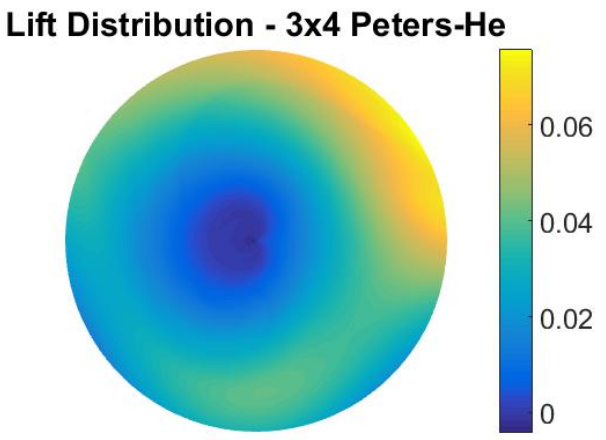

Fig. 18. Lift distribution using Peters-He Models at 10m/s

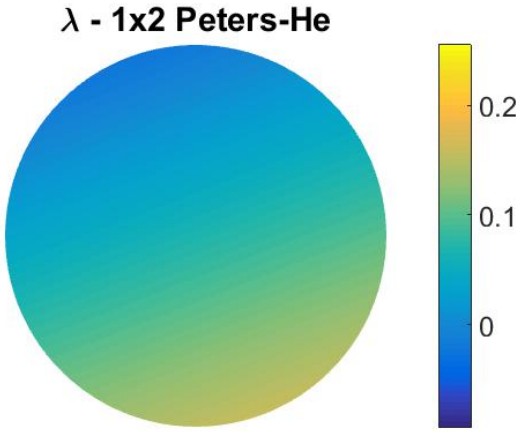

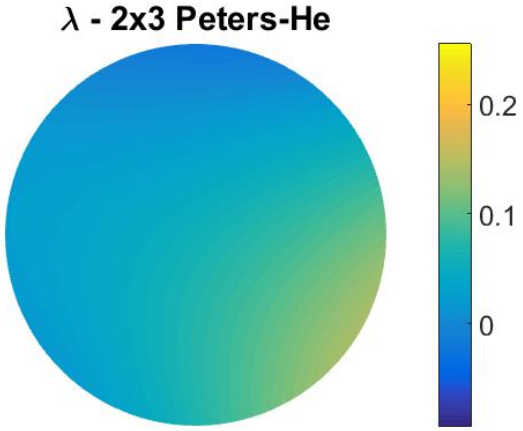

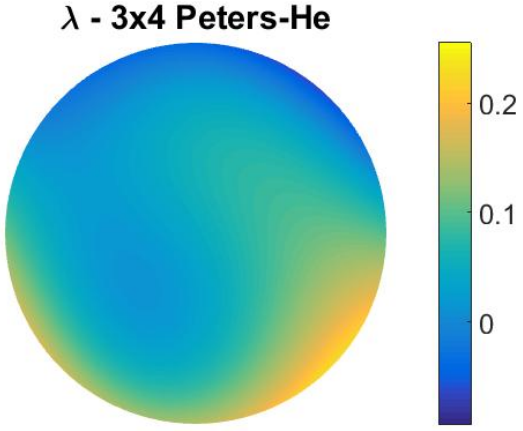

Fig. 19. Inflow distribution using Peters-He Models at 10 m/s

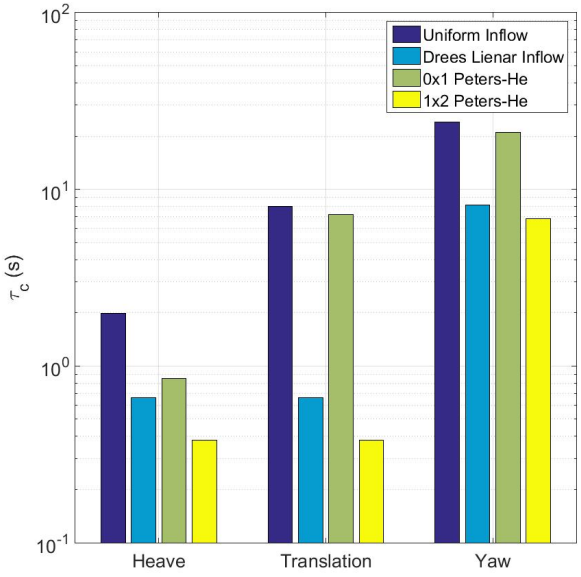

Fig. 20. Non-oscillatory Mode Time Constants - Hover

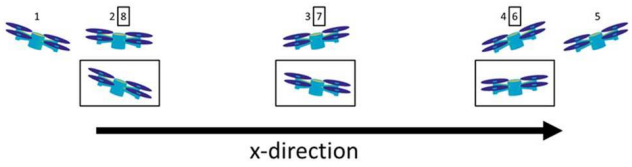

Fig. 21. Phugoid Mode in hover

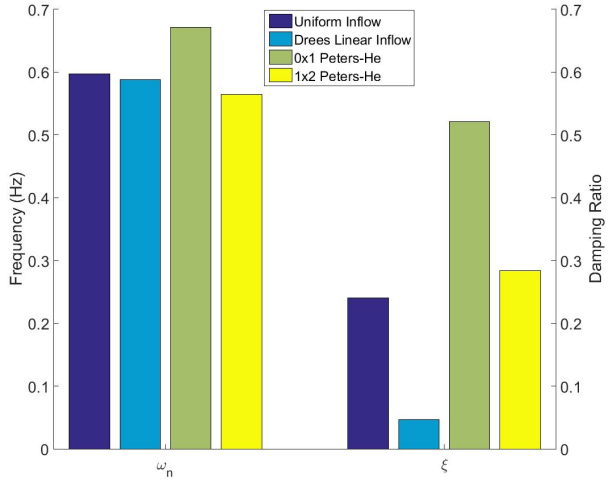

Fig. 22. Phugoid Mode Frequency and Damping ratio - hover

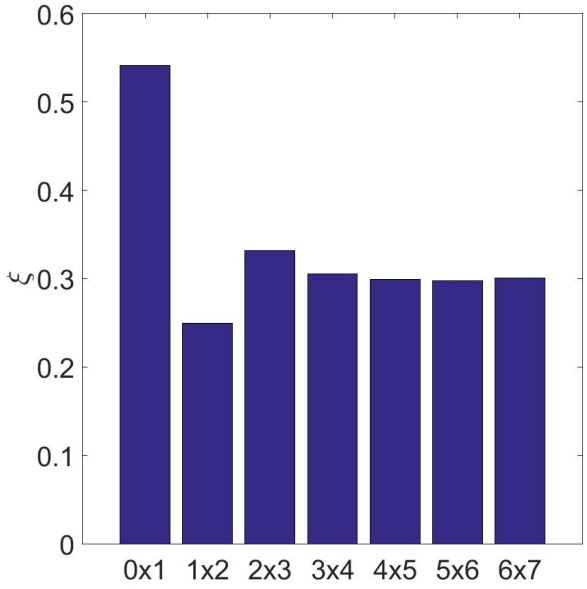

Fig. 23. Convergence of the damping ratio of the phugoid mode with higher order Peters-He Models